MPMI Vol. 38, No. 1, 2025, pp. 50–55, https://doi.org/10.1094/MPMI-09-24-0111-SC

SHORT COMMUNICATION

Redox Status-Selective Imaging of Iron in Vegetative and Pathogenic Fungal Cells Using Fluorescent Dyes Synthesized Via Simple Chemical Reactions

Lala Aliyeva-Schnorr,[1] Niels V. Heise,[2] René Csuk,[2] and Holger B. Deising[1,†]

[1] Phytopathologie und Pflanzenschutz, Institut für Agrar- und Ernährungswissenschaften, Martin-Luther-Universität Halle-Wittenberg, Halle (Saale), Germany

[2] Organische Chemie, Institut für Chemie, Martin-Luther-Universität Halle-Wittenberg, Halle (Saale), Germany

Accepted for publication 23 October 2024.

Iron plays a prominent role in various biological processes and is an essential element in almost all organisms, including plant-pathogenic fungi. As a transition element, iron occurs in two redox states, Fe^{2+} and Fe^{3+}, the transition between which generates distinct reactive oxygen species (ROS) such as H_2O_2, OH^- anions, and toxic OH· radicals. Thus, the redox status of Fe determines ROS formation in pathogen attack and plant defense and governs the outcome of pathogenic interactions. Therefore, spatially resolved visualization of Fe^{2+} and Fe^{3+} are essential to understand microbial pathogenesis. Here, we report a simple method for synthesis of the redox-state-selective dyes pyrene-tetramethyl piperidinyl oxyl (p-TEMPO) and 4-(4-methylpiperazine-1)-7-nitrobenz-2-oxa-1,3-diazole (MPNBD) for fluorescence microscopy-based imaging of Fe^{2+} and Fe^{3+} ions. Using these dyes, the occurrence and spatial distribution of Fe^{2+} and Fe^{3+} ions in vegetative and pathogenic hyphae of the hemibiotrophic maize anthracnose fungus *Colletotrichum graminicola* are shown.

Keywords: 1-hydroxy-2,2,6,6-tetramethyl-4-piperidinyl-1-pyrene carboxylate, 4-(4-methyl-1-piperazinyl)-7-nitro-2,1,3-benzoxadiazole, appressoria, *Colletotrichum graminicola*, iron, MPNBD, nuclei, p-TEMPO, vegetative development

Although iron is the fourth most abundant element on earth, its solubility and bioavailability in aerobic environments are extremely low, with less than 10^{-18} M at neutral pH (Schwyn and Neilands 1987). Despite its low bioavailability, iron plays an essential role in several biochemical reactions, including the generation of toxic reactive oxygen species (ROS) in plants and/or microbes and, moreover, the respiratory burst oxidase homolog-derived ROS function in wound responsiveness and plant development (Sagi et al. 2004). Highlighting the crucial importance of iron in the interaction between pathogenic fungi and plants, numerous papers have shown that defects in reductive or siderophore-mediated iron uptake strongly affect fungal virulence (Albarouki and Deising 2013; Albarouki et al. 2014; Haas et al. 2008). Depending on the predominant presence of Fe^{2+} or Fe^{3+}, distinct ROS such as H_2O_2, OH^- anions, and toxic OH· radicals are generated and used by plants to combat pathogens and by pathogens to kill host cells (Mehdy 1994). As Fe^{2+} has a higher solubility and exhibits greater bioactivity than Fe^{3+}, more pronounced cell damage can be anticipated to occur in the presence of Fe^{2+} ions (Winterbourn 1995). Accordingly, the availability of redox-state-selective iron dyes would significantly support the understanding of microbial virulence and plant defense. Interestingly, more than 25 years ago, a protocol allowing Fe^{2+} and Fe^{3+} ions in thin brain sections to be microscopically discriminated was developed in Alzheimer's disease research. That protocol includes incubation in ferricyanide or ferrocyanide for staining of Fe^{2+} or Fe^{3+}, respectively, and subsequent incubation in 3,3′-diaminobenzidine and H_2O_2 (Liu et al. 2007; Roschzttardtz et al. 2013; Smith et al. 1997). However, long processing times of 15 h and the fact that proof of Fe^{2+} and Fe^{3+} is only indirect represent clear disadvantages of this protocol.

A methodological breakthrough was the discovery that the two Fe^{2+}- and Fe^{3+}-specific fluorescent dyes pyrene-tetramethyl piperidinyl oxyl (p-TEMPO) and 7-(4-methylpiperazin-1)-4-nitrobenz-2-oxa-1,3-diazole (MPNBD) allow fast and direct redox status-specific visualization of Fe^{2+} and Fe^{3+} in plant tissue (Chen et al. 2006; Park et al. 2014).

Since these dyes are not commercially available, we optimized protocols for the synthesis of p-TEMPO and MPNBD. The synthesis of p-TEMPO fluorochromes started with the 1-ethyl-3-(3-dimethylaminopropyl) carbodiimide (EDC)-mediated reaction of pyrene-1-carboxylic acid with hydroxy-TEMPO in dry dichloromethane, yielding p-TEMPO (Fig. 1) at 87% isolated yield. The use of EDC was more efficient than the previously used dicyclohexylcarbodiimide, which yielded only 67%. In comparison with the EDC-mediated reaction, polymer-bound EDC resulted in a slightly lower yield of 81% (Chen et al. 2006; Ottaviani et al. 2001). MPNBD was synthesized from the reaction of 4-chloro-7-nitrofurazan and *N*-methylpiperazine in dry dichloromethane for 1 h at 22°C (Fig. 1), yielding 79% MPNBD as an orange amorphous solid (Park et al. 2014). For details of the synthetic procedure, the reader is referred to the supplementary materials.

We tested the fluorescent redox-status-selective dyes using conidia, vegetative hyphae, and in planta differentiated infection

†Corresponding author: H. B. Deising; holger.deising@landw.uni-halle.de

Funding: This work was supported by the State of Saxony-Anhalt (Landesschwerpunkt Sachsen-Anhalt, Project 2-5: The Trojan Horse-Strategy: An innovative method for controlling human and plant pathogenic fungi) to R. Csuk and H. B. Deising.

e-Xtra: Supplementary material is available online.

The author(s) declare no conflict of interest.

structures of the wild-type (WT) strain M2 (synonym M1.001) of the maize anthracnose fungus *Colletotrichum graminicola* (https://mycocosm.jgi.doe.gov/Colgr1/Colgr1.home.html; accessed on 15 April 2024). Falcate conidia taken from acervuli of 14-day-old colonies growing on oatmeal agar (OMA) (Werner et al. 2007) were directly stained with MPNBD or p-TEMPO (Fig. 2A, B, and E). To stain vegetative hyphae, a mycelial plug was inoculated onto potato dextrose agar (PDA) near a sterile glass coverslip and incubated at 23°C for 5 to 7 days, allowing hyphae to grow onto the glass surface. These hyphae were not contaminated with solidified agar medium, which improved the quality of fluorescence microscopy.

The staining solution used to detect Fe^{2+} ions contained 50 μM p-TEMPO in 0.2 M H_2SO_4 (Chen et al. 2006). To detect Fe^{3+} ions, 20 μM MPNBD was dissolved in ethanol (Park et al. 2014). Brightfield and fluorescence microscopy were performed using a Nikon Eclipse 600 microscope (Nikon, Düsseldorf, Germany). Digital images were taken using a DS-5M camera (Nikon, Düsseldorf, Germany), and the software package Lucia 4.61 (Nikon, Düsseldorf, Germany) was used for image processing. To confirm the presence of iron in hyphal cell walls and/or septae, hyphae were counterstained with the chitin/chitosan-binding fluorochrome Calcofluor White-M2R (CFW; Sigma-Aldrich, Steinheim, Germany), which was applied to the coverslip at 10-fold aqueous dilution of the commercial product and incubated for 5 min at room temperature. To confirm iron localization in nuclei and to avoid nuclear fluorescence overlapping with iron staining, two distinct nuclear stains were combined with MPNBD and p-TEMPO, respectively. MPNBD-stained nuclei were counterstained with the DNA-specific fluorescence dye 4′,6-diamidino-2-phenylindole (DAPI; 1 μg/ml, Roti Mount Flour Care, Carl Roth, Karlsruhe, Germany), and p-TEMPO staining was combined with GelRed-staining (300-fold diluted stock dilution; Sigma-Aldrich, Taufkirchen, Germany). For double staining of Fe^{2+} and Fe^{3+}, fungal structures were first stained with 50 μM p-TEMPO/0.2 M H_2SO_4 for 10 min, rinsed with double-distilled H_2O, stained with 20 μM MPNBD for 20 min at room temperature, and washed again with double-distilled H_2O. Fluorescence microscopy was performed using filter set R1 51 W (Nikon, Düsseldorf, Germany). For the detection of p-TEMPO fluorescence, an excitation wavelength of $\lambda = 358$ nm and a detection channel with a $\lambda = 461$ nm emission maximum were used. For the detection of MPNBD fluorescence, an excitation wavelength of $\lambda = 488$ nm and a $\lambda = 535/550$ nm detection channel were used. The filter combination UV-2A with an excitation wavelength of $\lambda = 330$ to 380 nm and Tx Red with an excitation wavelength of $\lambda = 330$ to 380 nm were used for the detection of Calcofluor and GelRed fluorochromes, respectively. Image acquisition was done using ImageJ (Schneider et al. 2012).

MPNBD staining revealed uniform labeling of Fe^{3+} in the cytoplasm of conidia and vegetative hyphae (Fig. 2A and B, arrow). Intriguingly, MPNBD staining also indicated that nuclei of conidia were loaded with Fe^{3+}, as confirmed by double-staining with DAPI (Fig. 2B and C, arrowheads). Vacuoles formed in vegetative hyphae did not exhibit fluorescence after MPNBD staining (Fig. 2I and J, arrowheads), suggesting that these compartments were devoid of Fe^{3+}. As compared with nuclei in conidia, nuclei present in vegetative hyphae fluoresced weakly or were not stained by MPNBD. Intriguingly, Fe^{3+} was associated with septae, as confirmed by double staining with Calcofluor (Fig. 2I to L, long white arrows). Importantly, fluorescence emission spectra of MPNBD and p-TEMPO did not overlap (Supplementary Fig. S1), allowing simultaneous dual staining of Fe^{2+} and Fe^{3+} (Fig. 2M). p-TEMPO-stained conidia and vegetative hyphae showed blue-fluorescing vacuoles, suggesting spatial separation of highly reactive Fe^{2+} from the cytoplasm (Fig. 2D to H, white and blue arrowheads). Staining of conidia with p-TEMPO and GelRed, a DNA dye emitting red fluorescence not interfering with the emission spectrum of p-TEMPO, did not show spatial signal overlaps, suggesting the absence of Fe^{2+} from nuclei (Fig. 2E, blue and red arrowheads). As a control, hyphae growing on medium containing 100 μM of the iron scavenger bathophenanthroline disulfonate (BPS; GFS Chemicals, Powell OH, U.S.A.) did not fluoresce with either of the iron redox status-specific dyes (Fig. 2N and O).

When inoculated onto hydrophobic surfaces like plant cuticles or poly-L-lysine-coated microscopy coverslips, conidia of many fungal pathogens, including the maize pathogen *C. graminicola*, differentiate melanized infection cells called appressoria (Chethana et al. 2021; Henson et al. 1999; Oliveira-Garcia et al. 2022).

Melanized appressoria (Fig. 3A, arrowhead) were neither stained by MPNBD nor by p-TEMPO (Fig. 3B and C, arrowheads). Failure of staining may be due to the fluorescence-scavenging activity of melanin and/or significant reduction of cell wall pore diameters by the inclusion of melanin into appressorial cell walls (Howard et al. 1991), making appressorial walls impermeable to these dyes. To generate nonmelanized appressoria, infection cells were allowed to form in the presence of the scytalone dehydratase and melanin biosynthesis inhibitor carpropamid (Kurahashi et al. 1998; Fig. 3D and I, arrowheads). In nonmelanized appressoria (Fig. 3D and I, arrowheads), MPNBD prominently labeled nuclei (Fig. 3E, arrowheads), as confirmed by DAPI counterstaining (Fig. 3F and G, arrows). Nuclei of nongerminated, but not of germinated conidia, fluoresced in the presence of MPNBD (Fig. 3E to G, arrows), and the vast majority of appressorial nuclei displayed strong fluorescence after MPNBD staining (Fig. 3E to G, arrowheads;

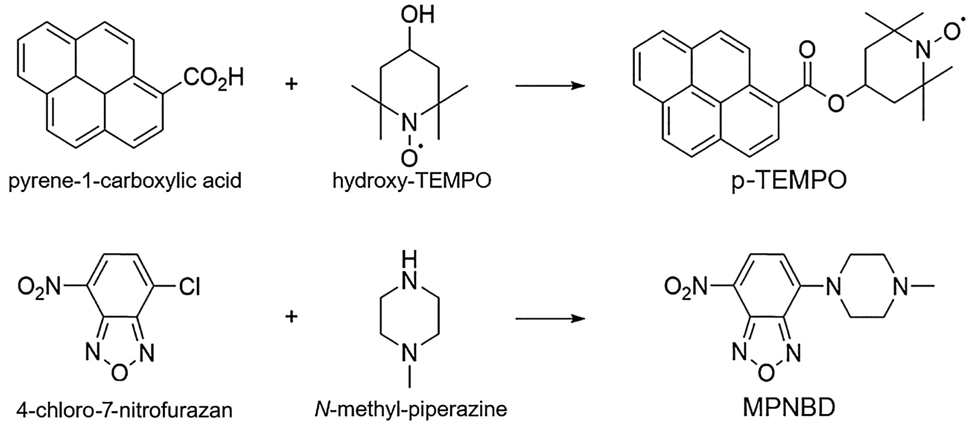

Fig. 1. Synthesis of the Fe^{2+}- and Fe^{3+}-selective fluorochromes pyrene-tetramethyl piperidinyl oxyl (p-TEMPO) and 4-(4-methylpiperazine-1)-7-nitrobenz-2-oxa-1,3-diazole (MPNBD). Pyrene-1-carboxylic acid and hydroxy-TEMPO were used for the synthesis of p-TEMPO, and MPNBD was synthesized through the reaction of 4-chloro-7-nitrofurazan and *N*-methyl-piperazine. For details, see the text.

Fig. 3H, app, green bar). By contrast, only some 30% of nuclei of vegetative hyphae fluoresced after MPNBD staining (Fig. 3H, vh, green bar), and fluorescence was weaker than that of appressorial nuclei (data not shown). p-TEMPO staining indicated the presence of Fe^{2+} in conidial and appressorial vacuoles (Fig. 3J and L, arrowheads), but p-TEMPO signals did not co-localize with nuclear fluorescence as indicated by GelRed staining (Fig. 3K and L, red arrows) and did thus not provide evidence for the presence of Fe^{2+} in appressorial nuclei (Fig. 3H). Thus, MPNBD staining suggests cell type-specific Fe^{3+} loading of nuclei.

In addition to the expediency of MPNBD and p-TEMPO for Fe^{3+} and Fe^{2+} localization in spores and surface-localized hyphae or infection cells, the dyes have been used to address the occurrence of these ions in pathogenic hyphae in planta. For maize infection assays, the youngest fully expanded leaf of 2- to 3-week-old maize plants (*Zea mays* cultivar Golden Jubilee; Territorial Seed Company, Cottage Grove, OR, U.S.A.) was used as described (Werner et al. 2007). The conidial density was adjusted to 5×10^5/ml in 0.02% (v/v) Tween 20, and 10-µl droplets were placed onto the midrib of the adaxial leaf surface. At 72 h postinoculation (hpi), the main vascular bundle was removed from the abaxial side, and staining solutions were applied and allowed to diffuse into the infected plant tissue. Microscopy revealed that appressoria (Fig. 4A and C, asterisks) and biotrophic (Fig. 4A and C, arrowheads) and necrotrophic pathogenic hyphae (Fig. 4A and C, arrows) had formed at that time point. MPNBD staining indicated the presence of Fe^{3+} in both biotrophic and necrotrophic hyphae (Fig. 4B, arrowheads and arrows). Intriguingly, maize cell walls also fluoresced intensively (Fig. 4B, empty five-pointed star). As in nonpathogenic vegetative hyphae, p-TEMPO staining suggested the presence of Fe^{2+} in vacuoles of pathogenic hyphae (Fig. 4D, blue

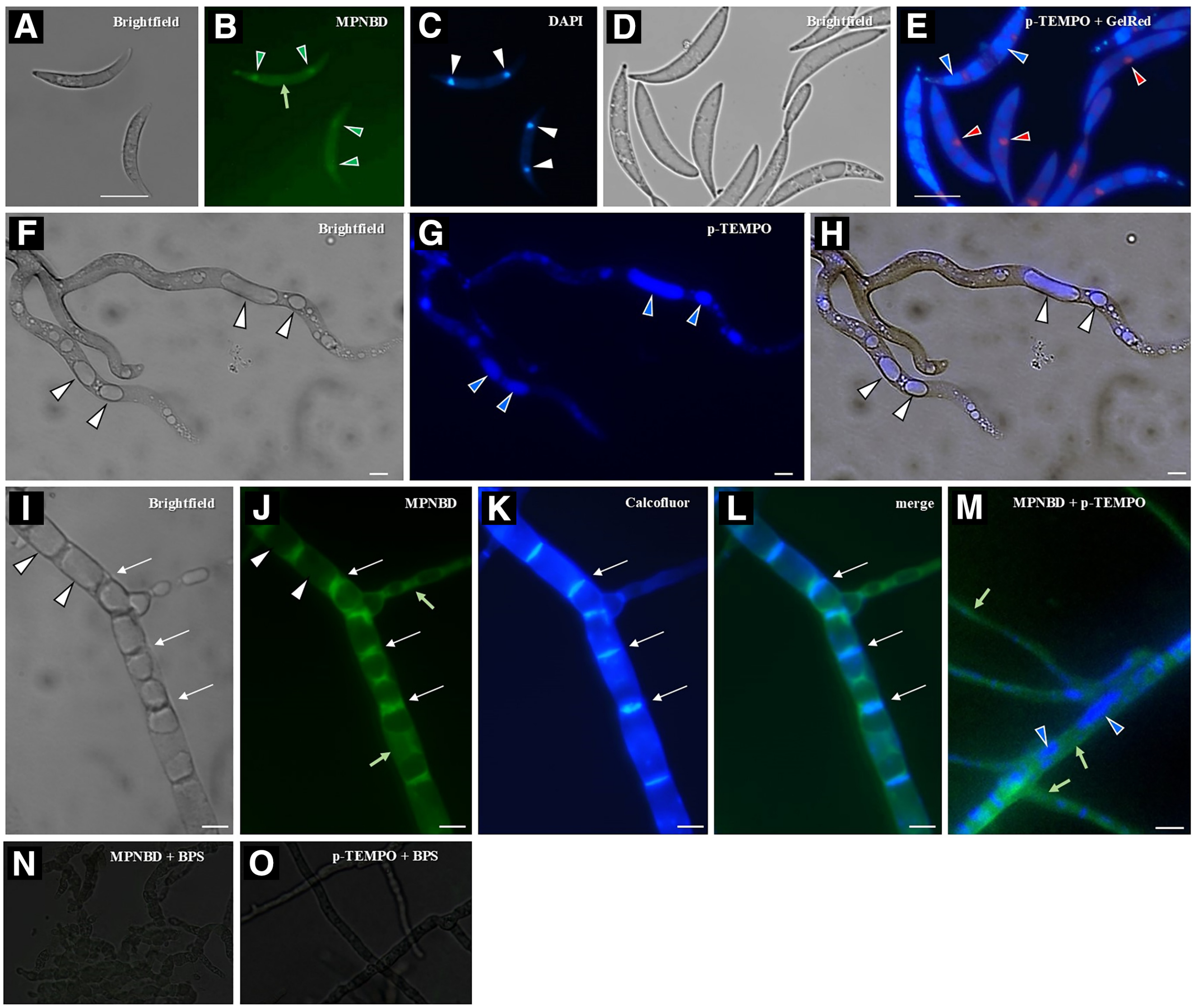

Fig. 2. Differential staining of spores and vegetative hyphae with pyrene-tetramethyl piperidinyl oxyl (p-TEMPO) and 4-(4-methylpiperazine-1)-7-nitrobenz-2-oxa-1,3-diazole (MPNBD). **A to C,** Double staining of conidia of *Colletotrichum graminicola* with MPNBD and 4′,6-diamidino-2-phenylindole (DAPI), showing localization of Fe^{3+} in nuclei. Green arrowheads and the arrow indicate Fe^{3+} in nuclei and in the cytoplasm. **D and E,** Double staining of conidia of *C. graminicola* with p-TEMPO and GelRed. Blue arrowheads point to Fe^{2+} in vacuoles, and red arrowheads mark nuclei. **F to H,** p-TEMPO staining of vegetative hyphae. Arrowheads indicate vacuoles. **I to L,** Double staining of vegetative hyphae with MPNBD and Calcofluor. White arrows point to septae with an overlapping Fe^{3+} profile; white arrowheads indicate iron-free vacuoles; short green arrows indicate iron in the cytoplasm. **M,** Double staining of the same hyphae with p-TEMPO (blue) and MPNBD (green); short green arrows show cytoplasmic Fe^{3+}, and blue arrowheads show Fe^{2+} in vacuoles. **N and O,** Fluorescence images overlaid upon brightfield images of vegetative hyphae grown in the presence of bathophenanthroline disulfonate (BPS). In the presence of BPS, hyphae were not stained by MPNBD or p-TEMPO. Scale bars = 10 µm.

arrowheads) as well as in plant cell walls (Fig. 4D, empty five-pointed star).

The transition between redox states is a key feature for a variety of iron-dependent biochemical reactions (Howard 1999; Lobreaux et al. 1992). As Fe^{2+} and Fe^{3+} play distinct roles in microbial plant infection (Haas et al. 2008; Misslinger et al. 2021; Stanford and Voigt 2020; Voß et al. 2020; Wu et al. 2023), the localization of and discrimination between Fe^{2+} and Fe^{3+} is of key importance for the understanding of microbial pathogenesis. Despite the important role of iron in pathogen-plant interactions, differential staining of Fe^{2+} and Fe^{3+} at the cellular level has rarely been accomplished (Albarouki and Deising 2013; Liu et al. 2007; Lobreaux et al. 1992; Misslinger et al. 2021; Roschzttardtz et al. 2013; Voß et al. 2020; Ye et al. 2014), primarily due to a lack of Fe^{2+}- and Fe^{3+}-specific probes for microscopy.

Previously, only DNAzyme-based catalytic beacon sensors allowed the simultaneous depiction of Fe^{2+} and Fe^{3+} ions. DNAzymes are fluorophore-conjugated DNA molecules that display enzymatic activities only in the presence of cofactors such as specific metal ions (Qian et al. 2010). Thus, the fluorophore is enzymatically released from redox-selective iron probes only in the presence of either Fe^{2+} or Fe^{3+}, and combinations of probes with fluorophores differing in emission spectra indeed allowed to optically discriminate between Fe^{2+} and Fe^{3+} (Wu et al. 2023). Thus, DNAzyme sensors allowed simultaneously visualizing Fe^{2+} and Fe^{3+} in brain slices of Alzheimer's disease mice and suggested that not only total iron but also iron redox cycling plays a key role in disease progression (Wu et al. 2023). However, the generation of DNAzyme sensors requires intricate molecular procedures and may therefore not be suitable for any lab.

Here, we report a simplified chemical method to synthesize redox state-selective dyes with nonoverlapping emission spectra for simple and rapid simultaneous imaging of Fe^{2+} and Fe^{3+}. Interestingly, the fluorescent dyes p-TEMPO and MPNBD permit individual as well as simultaneous imaging of Fe^{2+} and Fe^{3+}. p-TEMPO staining showed that in conidia and in vegetative and pathogenic fungal hyphae, highly reactive Fe^{2+} iron is restricted to vacuoles, which, plausibly, avoids toxic effects. Fe^{3+}, in contrast, was depicted in the cytosol and in association with septae, and MPNBD showed cell type-selective staining of nuclei in *C. graminicola*. Cell cycle-specific iron loading of nuclei has also been reported for human lymphocyte cells (Robinson et al. 2016; Zhang 2014). Interestingly, in both the rice blast fungus *Magnaporthe oryzae* and in the cucumber anthracnose fungus *C. lagenarium*, appressorium development and plant infection are strictly regulated by cell cycle progression (Fukada and Kubo 2015; Osés-Ruiz and Talbot 2017). Thus, it would be interesting to study the role of iron in cell cycle control in fungal pathogenesis, including the differentiation of appressoria and infection hypha formation in planta. The dyes introduced here may be useful to address this and related questions in pathogenesis.

In summary, we report on simple chemical methods to synthesize the redox status-selective fluorescent iron dyes p-TEMPO and MPNBD. Using conidia and vegetative and pathogenic hyphae of the maize pathogen *C. graminicola*, we demonstrate that this method combines the advantage of rapid redox status-selectivity visualization of iron with short processing times of less than 30 min.

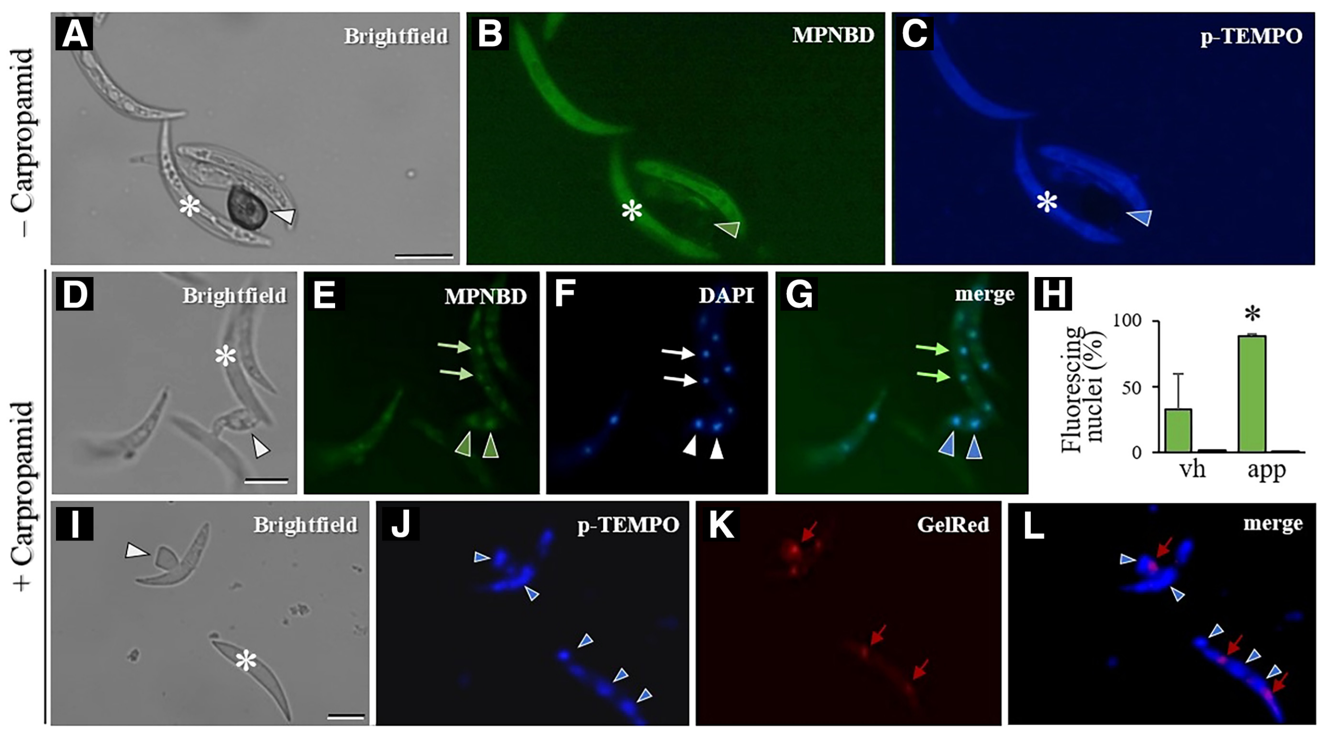

Fig. 3. Fluorescence labeling of Fe^{2+} and Fe^{3+} in conidia and appressoria of *Colletotrichum graminicola* differentiated in the absence (−) or presence (+) of carpropamid. **A to C,** Conidia and appressorium double-stained by 4-(4-methylpiperazine-1)-7-nitrobenz-2-oxa-1,3-diazole (MPNBD) and pyrene-tetramethyl piperidinyl oxyl (p-TEMPO). An asterisk indicates a nongerminated conidium, and the arrowhead points at a melanized appressorium. **D to G,** Conidia and nonmelanized appressorium double-stained with MPNBD and 4′,6-diamidino-2-phenylindole (DAPI) and merged images. Arrows and arrowheads indicate nuclei in nongerminated conidia and in the appressorium, respectively. G, The merge of E and F shows the presence of Fe^{3+} in nuclei of nongerminated conidia (arrows) and in the appressorium (arrowheads). **H,** Quantification of MPNBD (green bars)- and p-TEMPO-stained nuclei (blue bars) of vegetative hyphae (vh) and appressoria (app). **I to L,** Conidia and nonmelanized appressorium double-stained with p-TEMPO and GelRed. I, An asterisk indicates a conidium, and the arrowhead points to a nonmelanized appressorium. J and K, Arrowheads indicate Fe^{2+}-containing vacuoles, and arrows point to nuclei. L, The merged image shows that Fe^{2+} is not detected in nuclei. Scale bars = 10 µm.

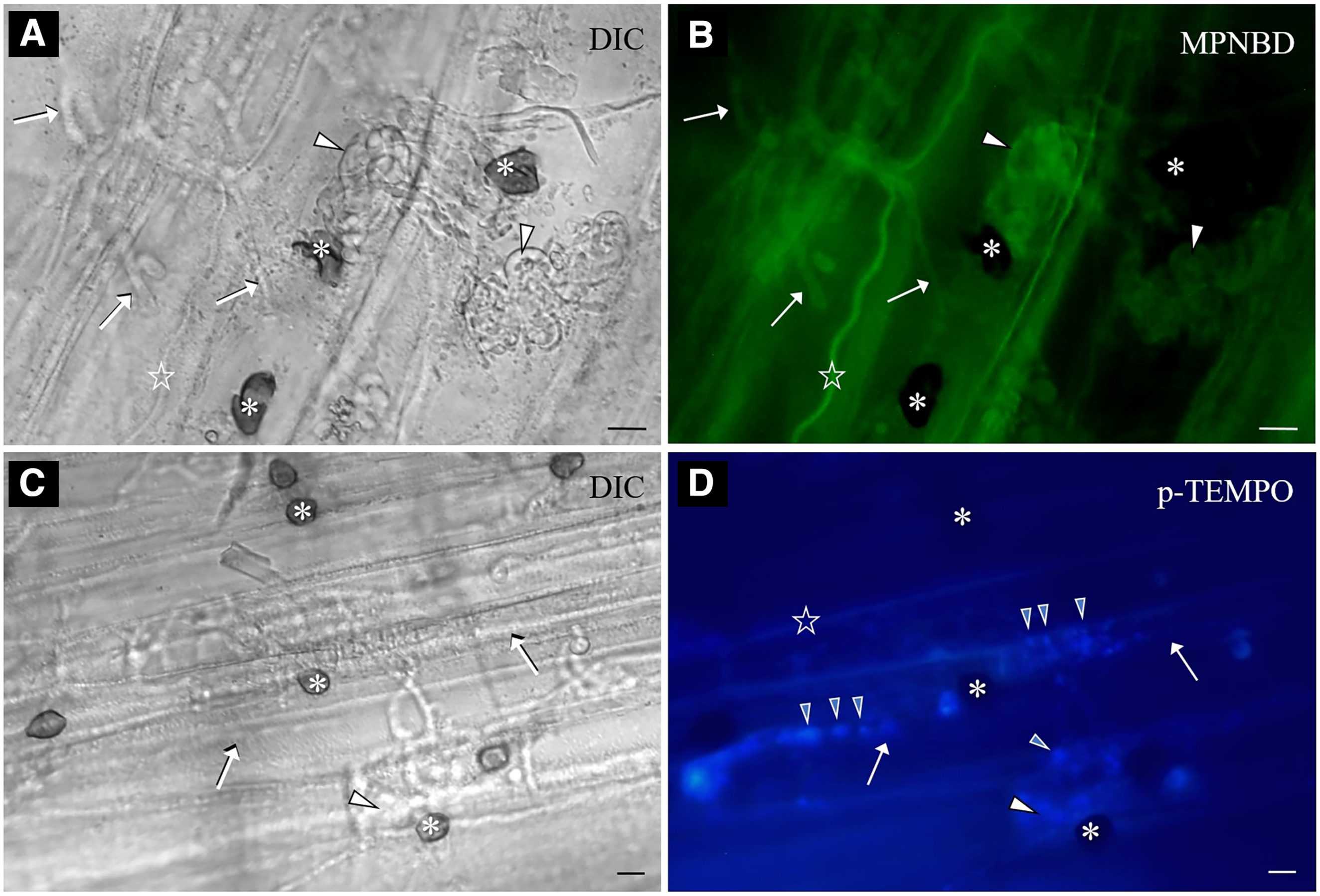

Fig. 4. Fluorescence labeling of Fe^{2+} and Fe^{3+} in biotrophic and necrotrophic hyphae of *Colletotrichum graminicola* formed in planta. **A to D,** After differentiation of an appressorium (DIC; asterisks), the fungus forms voluminous biotrophic primary (white arrowheads) and thin necrotrophic hyphae (arrows). B, 4-(4-methylpiperazine-1)-7-nitrobenz-2-oxa-1,3-diazole (MPNBD) labeling indicates the presence of Fe^{3+} in biotrophic and necrotrophic hyphae (arrowheads and arrows, respectively), as well as in the plant cell wall (open five-pointed star). D, Pyrene-tetramethyl piperidinyl oxyl (p-TEMPO) staining revealed the presence of Fe^{2+} in vacuoles (blue arrowheads) of biotrophic (white arrowhead) and necrotrophic (arrows) hyphae. Fe^{2+} was also detected in the maize cell wall (open five-pointed star). Scale bars = 10 μm.

Acknowledgments

Technical support by Elke Vollmer and help with initial experiments by Anja Raschke, Thea Stephan, and Immo Serbian is acknowledged. We are indebted to Edgar Peiter, Martin Luther University Halle-Wittenberg, for critical reading of and helpful comments on the manuscript.

Literature Cited

Albarouki, E., and Deising, H. B. 2013. Infection structure-specific reductive iron assimilation is required for cell wall integrity and full virulence of the maize pathogen *Colletotrichum graminicola*. Mol. Plant-Microbe Interact. 26:695-708.

Albarouki, E., Schafferer, L., Ye, F., von Wirén, N., Haas, H., and Deising, H. B. 2014. Biotrophy-specific downregulation of siderophore biosynthesis in *Colletotrichum graminicola* is required for modulation of immune responses of maize. Mol. Microbiol. 92:338-355.

Chen, J.-L., Zhuo, S.-J., Wu, Y.-Q., Fang, F., Li, L., and Zhu, C.-Q. 2006. High selective determination iron(II) by its enhancement effect on the fluorescence of pyrene-tetramethylpiperidinyl (TEMPO) as a spin fluorescence probe. Spectrochim. Acta A Mol. Biomol. Spectrosc. 63: 438-443.

Chethana, K. W. T., Jayawardena, R. S., Chen, Y.-J., Konta, S., Tibpromma, S., Abeywickrama, P. D., Gomdola, D., Balasuriya, A., Xu, J., Lumyong, S., and Hyde, K. D. 2021. Diversity and function of appressoria. Pathogens 10:746.

Fukada, F., and Kubo, Y. 2015. *Colletotrichum orbiculare* regulates cell cycle G1/S progression via a two-component GAP and a GTPase to establish plant infection. Plant Cell 27:2530-2544.

Haas, H., Eisendle, M., and Turgeon, B. G. 2008. Siderophores in fungal physiology and virulence. Annu. Rev. Phytopathol. 46:149-187.

Henson, J. M., Butler, M. J., and Day, A. W. 1999. The dark side of the mycelium: Melanins of phytopathogenic fungi. Annu. Rev. Phytopathol. 37:447-471.

Howard, D. H. 1999. Acquisition, transport, and storage of iron by pathogenic fungi. Clin. Microbiol. Rev. 12:394-404.

Howard, R. J., Ferrari, M. A., Roach, D. H., and Money, N. P. 1991. Penetration of hard substrates by a fungus employing enormous turgor pressures. Proc. Natl. Acad. Sci. U.S.A. 88:11281-11284.

Kurahashi, Y., Araki, Y., Kinbara, T., Pontzen, R., and Yamaguchi, I. 1998. Intermediates accumulation and inhibition sites of carpropamid in the melanin biosynthesis pathway of *Pyricularia oryzae*. J. Pestic. Sci. 23: 22-28.

Liu, G., Greenshields, D. L., Sammynaiken, R., Hirji, R. N., Selvaraj, G., and Wei, Y. 2007. Targeted alterations in iron homeostasis underlie plant defense responses. J. Cell Sci. 120:596-605.

Lobreaux, S., Massenet, O., and Briat, J.-F. 1992. Iron induces ferritin synthesis in maize plantlets. Plant Mol. Biol. 19:563-575.

Mehdy, M. C. 1994. Active oxygen species in plant defense against pathogens. Plant Physiol. 105:467-472.

Misslinger, M., Hortschansky, P., Brakhage, A. A., and Haas, H. 2021. Fungal iron homeostasis with a focus on *Aspergillus fumigatus*. Biochim. Biophys. Acta Mol. Cell Res. 1868:118885.

Oliveira-Garcia, E., Aliyeva-Schnorr, L., De Oliveira Silva, A., El Din Ghanem, S., Thor, K., Peiter, E., and Deising, H. B. 2022. The small Ras superfamily GTPase Rho4 of the maize anthracnose fungus *Colletotrichum graminicola* is required for β-1,3-glucan synthesis, cell wall integrity, and full virulence. J. Fungi 8:997.

Osés-Ruiz, M., and Talbot, N. J. 2017. Cell cycle-dependent regulation of plant infection by the rice blast fungus *Magnaporthe oryzae*. Commun. Integr. Biol. 10:e1372067.

Ottaviani, M. F., Venturi, F., Pokhrel, M. R., Schmutz, T., and Bossmann, S. H. 2001. Physicochemical studies on the adsorption properties of asbestos: 2. An EPR and fluorescence study on the adsorption of pyrene. J. Colloid Interface Sci. 238:371-380.

Park, M.-J., Jung, H.-S., Kim, Y.-J., Kwon, Y.-J., Lee, J.-K., and Park, C.-M. 2014. High-sensitivity fluorescence imaging of iron in plant tissues. Chem. Commun. 50:8547-8549.

Qian, X., Xiao, Y., Xu, Y., Guo, X., Qian, J., and Zhu, W. 2010. "Alive" dyes as fluorescent sensors: Fluorophore, mechanism, receptor and images in living cells. Chem. Commun. 46:6418-6436.

Robinson, I., Yang, Y., Zhang, F., Lynch, C., Yusuf, M., and Cloetens, P. 2016. Nuclear incorporation of iron during the eukaryotic cell cycle. J. Synchrotron Radiat. 23:1490-1497.

Roschzttardtz, H., Conéjéro, G., Divol, F., Alcon, C., Verdeil, J.-L., Curie, C., and Mari, S. 2013. New insights into Fe localization in plant tissues. Front. Plant Sci. 4:350.

Sagi, M., Davydov, O., Orazova, S., Yesbergenova, Z., Ophir, R., Stratmann, J. W., and Fluhr, R. 2004. Plant respiratory burst oxidase homologs impinge on wound responsiveness and development in *Lycopersicon esculentum*. Plant Cell 16:616-628.

Schneider, C. A., Rasband, W. S., and Eliceiri, K. W. 2012. NIH Image to ImageJ: 25 years of image analysis. Nat. Methods 9:671-675.

Schwyn, B., and Neilands, J. B. 1987. Universal chemical assay for the detection and determination of siderophores. Anal. Biochem. 160:47-56.

Smith, M. A., Harris, P. L. R., Sayre, L. M., and Perry, G. 1997. Iron accumulation in Alzheimer disease is a source of redox-generated free radicals. Proc. Natl. Acad. Sci. U.S.A. 94:9866-9868.

Stanford, F. A., and Voigt, K. 2020. Iron assimilation during emerging infections caused by opportunistic fungi with emphasis on Mucorales and the development of antifungal resistance. Genes 11: 1296.

Voß, B., Kirschhöfer, F., Brenner-Weiß, G., and Fischer, R. 2020. *Alternaria alternata* uses two siderophore systems for iron acquisition. Sci. Rep. 10:3587.

Werner, S., Sugui, J. A., Steinberg, G., and Deising, H. B. 2007. A chitin synthase with a myosin-like motor domain is essential for hyphal growth, appressorium differentiation, and pathogenicity of the maize anthracnose fungus *Colletotrichum graminicola*. Mol. Plant-Microbe Interact. 20:1555-1567.

Winterbourn, C. C. 1995. Toxicity of iron and hydrogen peroxide: The Fenton reaction. Toxicol. Lett. 82-83:969-974.

Wu, Y., Torabi, S.-F., Lake, R. J., Hong, S., Yu, Z., Wu, P., Yang, Z., Nelson, K., Guo, W., Pawel, G. T., Van Stappen, J., Shao, X., Mirica, L. M., and Lu, Y. 2023. Simultaneous Fe^{2+}/Fe^{3+} imaging shows Fe^{3+} over Fe^{2+} enrichment in Alzheimer's disease mouse brain. Sci. Adv. 9:eade7622.

Ye, F., Albarouki, E., Lingam, B., Deising, H. B., and von Wirén, N. 2014. An adequate Fe nutritional status of maize suppresses infection and biotrophic growth of *Colletotrichum graminicola*. Physiol. Plant. 151:280-292.

Zhang, C. 2014. Essential functions of iron-requiring proteins in DNA replication, repair and cell cycle control. Protein Cell 5:750-760.